

PIME: Prototype-based Interpretable MCTS-Enhanced Brain Network Analysis for Disorder Diagnosis

Kunyu Zhang¹, Yanwu Yang^{2✉}, Jing Zhang³, Xiangjie Shi⁴, and Shujian Yu^{5,6}

¹ Zhengzhou University, Zhengzhou, China

² University Hospital Tübingen, Tübingen, Germany
yangyanwu1111@gmail.com

³ China University of Geosciences, Wuhan, China

⁴ University of Science and Technology Beijing, Beijing, China

⁵ Vrije Universiteit Amsterdam, Amsterdam, The Netherlands

⁶ UiT - The Arctic University of Norway, Tromsø, Norway

Abstract. Recent deep learning methods for fMRI-based diagnosis have achieved promising accuracy by modeling functional connectivity networks. However, standard approaches often struggle with noisy interactions, and conventional post-hoc attribution methods may lack reliability, potentially highlighting dataset-specific artifacts. To address these challenges, we introduce PIME, an interpretable framework that bridges intrinsic interpretability with minimal-sufficient subgraph optimization by integrating prototype-based classification and consistency training with structural perturbations during learning. This encourages a structured latent space and enables Monte Carlo Tree Search (MCTS) under a prototype-consistent objective to extract compact minimal-sufficient explanatory subgraphs post-training. Experiments on three benchmark fMRI datasets demonstrate that PIME achieves state-of-the-art performance. Furthermore, by constraining the search space via learned prototypes, PIME identifies critical brain regions that are consistent with established neuroimaging findings. Stability analysis shows 90% reproducibility and consistent explanations across atlases.

Keywords: Explainable AI · fMRI · Brain disorder diagnosis · Information bottleneck · Prototype learning · Graph neural networks

1 Introduction

Brain disorders including autism spectrum disorder (ASD), Alzheimer’s disease (AD), and attention deficit hyperactivity disorder (ADHD) exhibit complex neural signatures, making precise neurobiological characterization challenging [15, 16, 22]. Resting-state functional magnetic resonance imaging (rs-fMRI) provides an in vivo, noninvasive window into brain function and has become a cornerstone of computational diagnostic frameworks. With the advent of deep learning, researchers have developed increasingly sophisticated models to analyze brain networks [24, 14]. Early convolutional neural networks captured localized functional

connectivity patterns, graph neural networks (GNNs) [1–3] advanced whole-brain relational modeling, and recent large-scale self-supervised methods [25] further improved diagnostic performance.

However, existing deep learning approaches face two critical limitations: processing whole-brain networks without modeling regional redundancy can be computationally inefficient and may overfit spurious connections, potentially degrading generalization and prediction stability; moreover, limited interpretability leaves clinicians unable to verify whether learned patterns reflect neurobiological mechanisms. The Information Bottleneck (IB) framework [7] addresses this by learning compressed representations that preserve task-relevant information and discard noise, as demonstrated by BrainIB [20] and BrainIB++ [21]. Prototype-based IB methods such as PGIB [11] further improve interpretability through case-based reasoning.

Despite these advances, existing explanations are still often expressed as soft attributions or masks and do not explicitly answer a clinically relevant question: which minimal set of brain regions is sufficient to preserve a diagnostic decision? In addition, many explanations lack a stable semantic anchor across subjects, making them vulnerable to dataset-specific artifacts rather than neurobiologically validated biomarkers.

To address this gap, PIME (**P**rototype-based **I**nterpretable **M**CTS-**E**nhanced Framework) combines prototype-based representation learning with post-training minimal-sufficient subgraph search. PIME promotes robust, distributed representations through consistency regularization with stochastic structural perturbations, and uses prototype consistency as a semantic anchor for explanation. This enables MCTS to identify compact explanatory subgraphs (typically 10 to 16 regions) that preserve model decisions while improving explanation stability.

Our contributions can be summarized as follows:

- We develop PIME, a unified framework that encourages robust representations via consistency training with structural perturbations, while integrating Information Bottleneck compression and prototype-based classification to improve noise sensitivity and interpretability.
- We introduce an MCTS-based post-training search guided by prototype similarity, operating on a structured latent space to identify compact explanatory subgraphs with neurobiologically plausible interpretations.
- Extensive evaluation on ABIDE, ADNI, and ADHD-200 demonstrates that PIME achieves state-of-the-art diagnostic accuracy (72.47% on leave-one-site-out autism classification) while identifying 10-16 critical regions that are consistent with established neuroimaging findings.

2 Related Work

2.1 MCTS for Interpretability

Unlike gradient-based methods that approximate importance via soft masks [33], search-based approaches treat interpretability as a combinatorial optimization

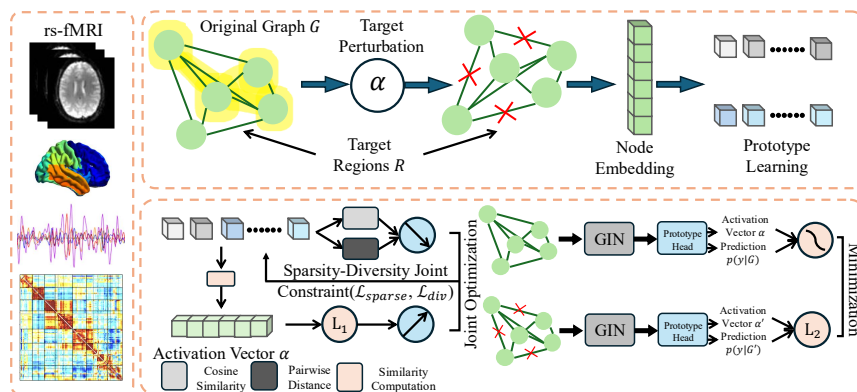


Fig. 1: Overview of the PIME framework. It consists of a prototype-based IB training pipeline with consistency regularization and a post-training MCTS module for explanatory subgraph extraction.

problem to identify exact subgraphs. Monte Carlo Tree Search (MCTS) has shown remarkable success in reinforcement learning [34] and recently in explaining graph models for molecular properties [35, 10]. By iteratively expanding search trees, MCTS can be less sensitive to local optima than gradient-based optimization in some settings. In neuroimaging, however, the search space is exponentially larger due to dense connectivity. PIME introduces a prototype-guided MCTS strategy for fMRI, using prototype similarity as high-level guidance to prune the search space and extract compact explanatory biomarkers.

3 Methodology

Figure 1 illustrates the architecture of PIME. Consider a dataset of brain recordings $\{\mathbf{X}_i, y_i\}_{i=1}^N$, where each recording $\mathbf{X}_i \in \mathbb{R}^{C \times T}$ represents the blood-oxygen-level-dependent (BOLD) signal from resting-state fMRI for the i -th patient. Here, C denotes the number of brain regions (e.g., 116 for AAL atlas [31] or 200 for CC200 atlas [32]), T indicates the temporal length, and $y_i \in \{1, \dots, K\}$ denotes the diagnostic label with K classes. From each BOLD signal \mathbf{X}_i , we compute a functional connectivity matrix $A_i \in \mathbb{R}^{C \times C}$ where each entry A_i^{jk} captures the Pearson correlation between brain regions j and k . We then construct a brain network $G_i = (V, A_i)$ where V represents C brain regions as nodes and A_i serves as the adjacency matrix. Our objective is to develop an interpretable classifier $f: G \rightarrow y$ that maps functional connectivity networks to diagnostic labels while identifying biologically meaningful biomarkers.

3.1 Information Bottleneck Prototype Learning

High-dimensional noise in fMRI networks necessitates compressed representations that preserve task-relevant information. Given a functional connectivity

network $G = (V, A)$ with C ROIs, we use a variational surrogate of the Information Bottleneck objective. The GIN encoder predicts a Gaussian posterior $p_\theta(Z|G) = \mathcal{N}(\boldsymbol{\mu}_\theta(G), \boldsymbol{\sigma}_\theta(G))$, and the compression term is implemented via KL divergence to a Gaussian prior:

$$\mathcal{L}_{IB} = \text{KL}(p_\theta(Z|G) \| r(Z)) \quad (1)$$

Unlike black-box neural networks, prototype-based classification enables interpretable predictions through case-based reasoning [17, 18]: classifications rely on similarity to learnable exemplars representing typical disease patterns, allowing clinicians to understand decisions by examining which prototypes activate for each patient.

We define M learnable prototypes $\mathcal{P} = \{\mathbf{p}_1, \dots, \mathbf{p}_M\}$ where $\mathbf{p}_k \in \mathbb{R}^d$ represents class-specific patterns [11]. Each prototype k is associated with learnable attention weights $\mathbf{a}_k \in \mathbb{R}^C$ that indicate the importance of each brain region for that prototype. A GIN encoder obtains graph embedding \mathbf{z} via reparameterization during training.

The similarity between the embedding and each prototype is measured using the squared Euclidean distance:

$$d_k(\mathbf{z}) = \|\mathbf{z} - \mathbf{p}_k\|_2^2 \quad (2)$$

The prototype activation is then computed via a softmax over negative distances:

$$s_k(\mathbf{z}) = \frac{\exp(-d_k(\mathbf{z}))}{\sum_{j=1}^M \exp(-d_j(\mathbf{z}))} \quad (3)$$

Let $\mathbf{s}(\mathbf{z}) = [s_1(\mathbf{z}), \dots, s_M(\mathbf{z})]^\top$. The predictive distribution is

$$P(y|G) = \text{softmax}(W \mathbf{s}(\mathbf{z}) + b). \quad (4)$$

The cross-entropy loss is

$$\mathcal{L}_{ce} = -\frac{1}{N} \sum_{i=1}^N \log P(y_i|G_i). \quad (5)$$

The prediction loss combines Cross-Entropy with prototype clustering and separation:

$$\mathcal{L}_{pred} = \mathcal{L}_{ce} + \lambda_1 \frac{1}{N} \sum_{i=1}^N \min_{k \in \mathcal{P}_{y_i}} d_k(\mathbf{z}_i) + \lambda_2 \frac{1}{N} \sum_{i=1}^N \max \left(0, \Delta - \min_{k \notin \mathcal{P}_{y_i}} d_k(\mathbf{z}_i) \right). \quad (6)$$

The second and third terms encourage samples to stay close to their class prototypes while remaining separated from other-class prototypes. The base objective is $\mathcal{L}_{base} = \mathcal{L}_{pred} + \beta \mathcal{L}_{IB}$.

3.2 Consistency Training and Regularization

To reduce sensitivity to localized artifacts and encourage perturbation-invariant representations, we adopt consistency regularization with stochastic structural perturbations. For each graph G_i , we uniformly sample without replacement a node subset $\mathcal{R}_{rand}^{(i)} \subset \{1, \dots, C\}$ with $|\mathcal{R}_{rand}^{(i)}| = \lfloor r \cdot C \rfloor$. The binary mask $\mathbf{M}_{rand}^{(i)} \in \{0, 1\}^{C \times C}$ is defined by $(\mathbf{M}_{rand}^{(i)})_{uv} = 1$ iff $u \in \mathcal{R}_{rand}^{(i)}$ or $v \in \mathcal{R}_{rand}^{(i)}$. The perturbed adjacency matrix is generated as $A_{i,pert} = A_i \odot (\mathbf{1} - \mathbf{M}_{rand}^{(i)})$, and the corresponding perturbed graph is $G_{i,pert} = (V, A_{i,pert})$.

To balance diagnostic accuracy with interpretability and stability under perturbations, we optimize:

$$\min_{\theta} \mathcal{L}_{total} = \mathcal{L}_{base} + \mathcal{R}(\theta) \quad (7)$$

The regularization term $\mathcal{R}(\theta)$ combines structural consistency and geometric constraints:

$$\begin{aligned} \mathcal{R}(\theta) = & \lambda_{cons} (\text{KL}(P(y|G) \| P(y|G_{pert})) + \|\mathbf{s}(G) - \mathbf{s}(G_{pert})\|_2^2) \\ & + \lambda_{sparse} \frac{1}{M} \sum_{k=1}^M \|\mathbf{a}_k\|_1 - \lambda_{div} \frac{1}{M(M-1)} \sum_{i \neq j} \|\mathbf{p}_i - \mathbf{p}_j\|_2^2 \end{aligned} \quad (8)$$

where λ_{cons} , λ_{sparse} , and λ_{div} control the strength of consistency, attention sparsity, and prototype diversity, respectively. With a slight abuse of notation, $\mathbf{s}(G)$ denotes $\mathbf{s}(\mathbf{z}(G))$. Both $P(y|G_{pert})$ and $\mathbf{s}(G_{pert})$ are computed by forwarding $G_{i,pert}$ through the same encoder and prototype classification head used for G_i . The consistency term penalizes the discrepancy between the predictions and prototype activations of the original and perturbed graphs, encouraging invariance to structural perturbations rather than reliance on a small set of potentially brittle connections. The sparsity term applies L_1 regularization to the prototype attention weights \mathbf{a}_k to encourage compact, human-interpretable region weighting. Finally, the diversity term increases pairwise distances between prototypes to reduce mode collapse and promote distinct prototype representations.

Post-training, we use MCTS to extract compact explanatory subgraphs by iteratively removing brain regions and scoring candidate subsets based on prototype similarity:

$$\text{score}(\mathcal{C}) = \log \left(\frac{d(\mathbf{z}_{\mathcal{C}}, \mathbf{p}^*) + 1}{d(\mathbf{z}_{\mathcal{C}}, \mathbf{p}^*) + \epsilon} \right) \quad (9)$$

where \mathcal{C} denotes the retained regions, $\mathbf{z}_{\mathcal{C}}$ is the masked graph embedding, and \mathbf{p}^* is the predicted prototype. Since $\text{score}(\mathcal{C})$ is monotonically decreasing in $d(\mathbf{z}_{\mathcal{C}}, \mathbf{p}^*)$ (for $0 < \epsilon < 1$), maximizing it favors subsets whose embeddings remain close to the predicted prototype. MCTS returns the selected regions in \mathcal{C}^* as the explanatory set under this objective.

Table 1: Comparison with baselines on fMRI-based diagnosis. All values represent classification accuracy (%). All shows mean \pm std over leave-one-site-out or 5-fold CV. ADNI and ADHD-200 use 5-fold CV. ADNI tasks: 3-class (NC/MCI/AD classification), NC vs AD, MCI vs AD, and NC vs MCI. Best in bold, second-best underlined.

Method	ABIDE	ADNI			ADHD-200	
		3-class	NC vs AD	MCI vs AD	NC vs MCI	
GCN [1]	63.48 \pm 7.61	58.27 \pm 5.43	72.94 \pm 4.72	71.63 \pm 4.86	66.13 \pm 5.21	63.72 \pm 1.84
GAT [2]	67.92 \pm 6.96	59.63 \pm 5.18	72.19 \pm 4.59	71.95 \pm 4.71	66.28 \pm 5.03	67.59 \pm 1.52
GIN [3]	67.84 \pm 6.79	60.12 \pm 5.07	73.01 \pm 4.51	72.68 \pm 4.63	68.33 \pm 4.89	67.81 \pm 1.61
Graph Transformer [5]	69.31 \pm 6.53	59.37 \pm 5.26	72.74 \pm 4.68	72.79 \pm 4.75	68.17 \pm 5.12	69.38 \pm 1.31
BrainNetTF [4]	<u>71.43</u> \pm 4.67	<u>65.18</u> \pm 4.47	<u>78.42</u> \pm 3.83	<u>77.56</u> \pm 4.01	<u>72.89</u> \pm 4.23	<u>71.28</u> \pm 1.21
SIB [19]	61.73 \pm 8.12	61.85 \pm 4.81	75.23 \pm 4.23	74.61 \pm 4.37	70.12 \pm 4.65	61.84 \pm 2.13
DIR-GNN [8]	66.82 \pm 6.18	62.17 \pm 4.73	75.81 \pm 4.15	74.36 \pm 4.29	70.63 \pm 4.58	66.71 \pm 1.73
ProtGNN [9]	64.51 \pm 6.71	63.16 \pm 4.62	76.49 \pm 4.08	76.19 \pm 4.21	71.59 \pm 4.47	64.68 \pm 1.89
PGIB [11]	64.37 \pm 6.74	61.71 \pm 4.69	75.24 \pm 4.11	75.19 \pm 4.35	71.01 \pm 4.51	64.82 \pm 1.96
BrainIB [20]	70.22 \pm 5.87	64.72 \pm 4.51	77.26 \pm 3.97	76.70 \pm 4.13	72.47 \pm 4.35	70.28 \pm 1.42
BrainIB++ [21]	70.63 \pm 5.68	64.29 \pm 4.56	78.13 \pm 3.89	77.19 \pm 4.08	72.61 \pm 4.29	70.73 \pm 1.28
PIME (Ours)	72.47\pm5.12	66.73\pm4.38	78.96\pm3.76	78.03\pm3.91	73.02\pm4.17	72.16\pm1.14

Table 2: Ablation study on key components. All values represent classification accuracy (%). Each variant removes one component while keeping others.

Dataset	w/o IB	w/o Proto	w/o Cons	w/o Sparse	w/o Div	Baseline	Full
ABIDE	70.10 \pm 5.28	61.72 \pm 6.43	67.54 \pm 5.67	68.86 \pm 5.41	70.57 \pm 5.19	63.98 \pm 6.21	72.47\pm5.12
ADNI (3-class)	63.18 \pm 4.52	57.39 \pm 5.67	61.52 \pm 4.89	62.87 \pm 4.63	64.05 \pm 4.47	59.21 \pm 5.41	66.73\pm4.38
ADHD-200	69.83 \pm 1.26	61.54 \pm 1.89	67.28 \pm 1.53	68.79 \pm 1.37	70.42 \pm 1.21	64.37 \pm 1.76	72.16\pm1.14

4 Experiments and Results

4.1 Datasets and Experimental Settings

We evaluate on three public fMRI datasets. ABIDE [26] contains 505 controls and 530 autism subjects. ADNI [27] contains 94 controls, 100 MCI, and 90 Alzheimer’s subjects. ADHD-200 [28] contains 364 controls and 218 ADHD subjects. Following standard preprocessing protocols [29, 30], brain regions are parcellated using AAL templates for ABIDE and ADHD-200, and CC200 templates for ADNI. Functional connectivity networks are constructed by computing Pearson correlation coefficients between all pairs of ROI time series from BOLD signals. We retain only the top 30% strongest connections to reduce noise and computational cost, forming a sparse adjacency matrix A .

All experiments use PyTorch on NVIDIA A100 GPUs with a 3-layer GIN encoder having hidden dimensions of 128, 256, and 512, and latent dimension $d = 64$. Training employs Adam optimization with learning rate 10^{-3} , decay rate 0.5 every 50 epochs, and weight decay 0.03 for 200 epochs with batch size 32. The number of prototypes is $M = 7C$ where C denotes the number of classes, yielding $M = 14$ for binary tasks and $M = 21$ for three-class ADNI. During consistency training, we randomly perturb $r = 25\%$ of brain regions. Hyperparameters are selected via grid search over $\lambda_1, \lambda_2, \lambda_{cons}, \lambda_{sparse}, \lambda_{div} \in$

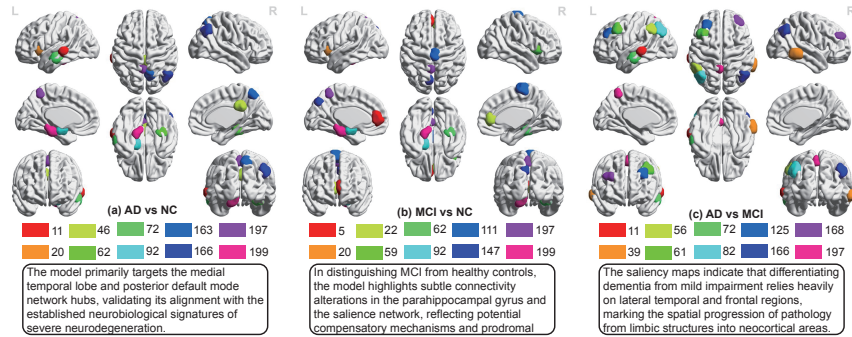


Fig. 2: Top 10 MCTS-identified critical brain regions for each diagnostic task. (a) ADNI AD vs NC. (b) ADNI MCI vs NC. (c) ADNI AD vs MCI.

$\{0.001, 0.01, 0.1\}$ and $\beta \in \{10^{-3}, 10^{-2}, 10^{-1}\}$, yielding $\beta = 0.001$, $\lambda_1 = \lambda_2 = 0.1$, $\lambda_{cons} = 0.1$, $\lambda_{sparse} = \lambda_{div} = 0.01$, $\Delta = 1.0$. MCTS uses 20 rollouts with score constant $\epsilon = 10^{-6}$. Competing models use their recommended hyperparameters.

4.2 Experimental Results and Ablation Study

We compare PIME with GNN backbones, Transformer baselines, and interpretable methods (see Table 1). All methods are evaluated using leave-one-site-out cross-validation on ABIDE and 5-fold cross-validation on ADNI and ADHD-200.

PIME consistently outperforms state-of-the-art methods across all benchmarks. On ABIDE and ADHD-200, our approach surpasses BrainIB++ by 1.84% and 1.43%, respectively. On ADNI, PIME achieves top performance in three-class staging (66.73%) and early MCI detection (73.02%) with superior stability.

Ablation studies systematically remove individual components to assess their contributions (Table 2). Prototype learning serves as the primary discriminative backbone, capturing the most critical class-specific patterns. The framework naturally fuses this with consistency training and Information Bottleneck regularization to enforce distributed biomarkers and filter high-dimensional noise, while diversity and sparsity constraints further refine feature distinctiveness, thereby consistently enhancing classification performance across all benchmarks.

4.3 MCTS-Based Interpretability Analysis

We apply MCTS post-training to extract compact explanatory subgraphs by iteratively pruning brain regions while monitoring prototype-guided prediction quality (Section 3.2). In practice, MCTS typically selects about 10 regions out of 116 and about 16 regions out of 200 ROIs. Importantly, this compactness reflects

Table 3: Top-5 activated regions per prototype (ADNI). Representative prototypes: P1-3 (NC), P8-10 (MCI).

Prototype	Rank 1	Rank 2	Rank 3	Rank 4	Rank 5
P1 (NC)	DMN: Precuneus L	DMN: Precuneus R	Visual: Calcarine R	Visual: Lingual L	DMN: Cuneus L
P2 (NC)	Motor: SMA R	Motor: Precentral L	Motor: Postcentral R	Auditory: Heschl L	Control: Parietal Inf
P3 (NC)	Visual: Occipital Mid	Visual: Fusiform L	DMN: PCC	Control: Frontal Mid	Visual: Calcarine L
P8 (MCI)	Limbic: ParaHippo R	Limbic: Hippo L	Limbic: ParaHippo L	Visual: Fusiform R	Temporal: Pole Mid
P9 (MCI)	SN: Insula L	SN: Insula R	SN: ACC L	SN: ACC R	Control: Frontal Inf
P10 (MCI)	SN: ACC R	Limbic: Amygdala L	SN: Frontal Med Orb	Subcortical: Thalamus	SN: Insula L

Table 4: Stability analysis.

(a) Reproducibility of MCTS-identified functional regions across different prototype numbers

Category	ADNI ROI IDs	ADHD ROI IDs
Shared Regions	5, 20, 22, 59, 62, 92, 147, 197, 199	29, 47, 49, 50, 51, 79, 80, 83, 92
M=14 Only	111	86
M=28 Only	121	85
Jaccard Similarity	90%	90%

(b) Cross-atlas stability on the same ADNI subjects

Method	Similarity
BrainIB	30%
BrainIB++	60%
PIME	80%

an operational minimal-evidence explanation under our scoring objective: it identifies a small subset of regions sufficient to preserve the model’s prototype-based decision, rather than implying that neurobiological mechanisms are intrinsically sparse or non-distributed.

Figure 2 visualizes the top-10 regions returned by MCTS for three binary classification tasks on ADNI. Starting from the full network, MCTS iteratively removes regions and evaluates the remaining subgraph via prototype-based prediction quality, returning a compact set of regions that best preserves the model’s decision under the objective in Eq. 9.

4.4 Prototype Activation Patterns and Stability Analysis

We analyze top-5 activated regions for ADNI prototypes (MCI vs. NC) by mapping ROIs to dominant anatomy (Table 3): NC prototypes emphasize posterior DMN and sensorimotor hubs, while MCI prototypes emphasize medial temporal and salience regions. Stability tests across prototype settings ($M = 14$ vs. 28) show 90% Jaccard similarity on ADNI and ADHD-200 (Table 4a), and Table 4b shows cross-atlas stability on the same ADNI subset (MCI, $n = 38$; NC, $n = 37$); for CC200, each ROI is mapped to the anatomical region with the largest weight contribution.

5 Conclusion and Future Work

In summary, PIME unifies prototype-based IB learning with MCTS to bridge accurate fMRI diagnosis and reliable, minimal-sufficient explanations. Across three

benchmarks, it achieves strong performance while extracting compact biomarkers (10–16 regions) with high reproducibility and cross-atlas consistency. Future work will develop multimodal prototype spaces and validate clinical robustness in prospective, multi-center settings.

References

1. Kipf, T.N., Welling, M.: Semi-supervised classification with graph convolutional networks. arXiv preprint arXiv:1609.02907 (2016)
2. Veličković, P., Cucurull, G., Casanova, A., Romero, A., Liò, P., Bengio, Y.: Graph attention networks. In: International Conference on Learning Representations (2018)
3. Xu, K., Hu, W., Leskovec, J., Jegelka, S.: How powerful are graph neural networks? arXiv preprint arXiv:1810.00826 (2018)
4. Kan, X., Dai, W., Cui, H., Zhang, Z., Guo, Y., Yang, C.: Brain network transformer. In: Advances in Neural Information Processing Systems, vol. 35, pp. 25586–25599. Curran Associates, Inc. (2022)
5. Shi, M., Zhang, S., Zhang, J., Wang, Q.: Masked label prediction: Unified message passing model for semi-supervised classification. In: Proceedings of the 29th International Joint Conference on Artificial Intelligence (IJCAI), pp. 1477–1483 (2020)
6. Yu, S., Jenssen, R., Principe, J.C.: Understanding convolutional neural networks with information theory: An initial exploration. IEEE Transactions on Neural Networks and Learning Systems 32(1), 435–442 (2020)
7. Tishby, N., Zaslavsky, N.: Deep learning and the information bottleneck principle. In: 2015 IEEE Information Theory Workshop (ITW), pp. 1–5. IEEE (2015)
8. Wu, Y., Wang, X., Zhang, A., He, X., Chua, T.S.: Discovering invariant rationales for graph neural networks. In: International Conference on Learning Representations (2022)
9. Zhang, Y., Defazio, D., Ramesh, A.: ProtGNN: Towards self-explaining graph neural networks. In: Proceedings of the AAAI Conference on Artificial Intelligence, vol. 36, pp. 9127–9135 (2022)
10. Wang, Y., Fan, S., Wang, M., Gao, S., Wang, C., Yin, N.: DAMR: Efficient and Adaptive Context-Aware Knowledge Graph Question Answering with LLM-Guided MCTS. In: The Fourteenth International Conference on Learning Representations (ICLR) (2026)
11. Seo, S., Kim, S., Park, C.: Interpretable prototype-based graph information bottleneck. Advances in Neural Information Processing Systems 36, 76737–76748 (2023)
12. Nauta, M., Schlötterer, J., Van Keulen, M., Seifert, C.: Pip-net: Patch-based intuitive prototypes for interpretable image classification. In: Proceedings of the IEEE/CVF Conference on Computer Vision and Pattern Recognition, pp. 2744–2753 (2023)
13. Gallée, L., Beer, M., Götz, M.: Interpretable medical image classification using prototype learning and privileged information. In: International Conference on Medical Image Computing and Computer-Assisted Intervention, pp. 435–445. Springer (2023)
14. Qiu, X., Wang, F., Sun, Y., Lian, C., Ma, J.: Towards graph neural networks with domain-generalizable explainability for fMRI-Based brain disorder diagnosis. In: International Conference on Medical Image Computing and Computer-Assisted Intervention, pp. 454–464. Springer (2024)

15. Jiang, Y., Wang, J., Zhou, E., Palaniyappan, L., Luo, C., Ji, G., Yang, J., Wang, Y., et al.: Neuroimaging biomarkers define neurophysiological subtypes with distinct trajectories in schizophrenia. *Nature Mental Health* 1(3), 186–199 (2023)
16. Yu, G., Liu, Z., Wu, X., et al.: Common and disorder-specific cortical thickness alterations in internalizing, externalizing and thought disorders during early adolescence: An Adolescent Brain and Cognitive Development Study. *Journal of Psychiatry and Neuroscience* 48(5), E345–E356 (2023)
17. Zhang, K., Wang, M., Shi, X., Xu, H., Zhang, C.: EVA-Net: Interpretable brain age prediction via continuous aging prototypes from EEG. *arXiv preprint arXiv:2511.15393* (2025)
18. Wang, Y., Zhang, K., Huang, J., Yin, N., Liu, S., Segal, E.: ProtoMol: Enhancing molecular property prediction via prototype-guided multimodal learning. *Briefings in Bioinformatics* 26(6), bbaf629 (2025)
19. Yu, J., Xu, T., Rong, Y., Bian, Y., Huang, J., He, R.: Recognizing predictive substructures with subgraph information bottleneck. *IEEE Transactions on Pattern Analysis and Machine Intelligence* 46(3), 1650–1663 (2021)
20. Zheng, K., Yu, S., Li, B., Jenssen, R., Chen, B.: BrainIB: Interpretable brain network-based psychiatric diagnosis with graph information bottleneck. *IEEE Transactions on Neural Networks and Learning Systems* (2024)
21. Hu, T., Li, Q., Liu, S., Calhoun, V.D., van Wingen, G., Yu, S.: BrainIB++: Leveraging graph neural networks and information bottleneck for functional brain biomarkers in schizophrenia. *Biomedical Signal Processing and Control* 112, 108803 (2026)
22. Zhang, K., Li, Q., Yu, S.: MvHo-IB: Multi-view higher-order information bottleneck for brain disorder diagnosis. In: *International Conference on Medical Image Computing and Computer-Assisted Intervention*, pp. 407–417. Springer (2025)
23. Wang, Y., Liang, V., Yin, N., Liu, S., Segal, E.: SGAC: a graph neural network framework for imbalanced and structure-aware AMP classification. *Briefings in Bioinformatics* 27(1), bbag038 (2026)
24. Yang, Y., Ye, C., Guo, X., Wu, T., Xiang, Y., Ma, T.: Mapping multi-modal brain connectome for brain disorder diagnosis via cross-modal mutual learning. *IEEE Transactions on Medical Imaging* 43(1), 108–121 (2023)
25. Yang, Y., Ye, C., Su, G., Zhang, Z., Chang, Z., Chen, H., Chan, P., Yu, Y., Ma, T.: Brainmass: Advancing brain network analysis for diagnosis with large-scale self-supervised learning. *IEEE Transactions on Medical Imaging* 43(11), 4004–4016 (2024)
26. Di Martino, A., Yan, C.G., Li, Q., et al.: The autism brain imaging data exchange: towards a large-scale evaluation of the intrinsic brain architecture in autism. *Molecular Psychiatry* 19(6), 659–667 (2014)
27. Jack Jr, C.R., Bernstein, M.A., Fox, N.C., et al.: The Alzheimer’s disease neuroimaging initiative (ADNI): MRI methods. *Journal of Magnetic Resonance Imaging* 27(4), 685–691 (2008)
28. Bellec, P., Chu, C., Chouinard-Decorte, F., Benhajali, Y., Margulies, D.S., Craddock, R.C.: The neuro bureau ADHD-200 preprocessed repository. *NeuroImage* 144, 275–286 (2017)
29. Cai, L., Zeng, W., Chen, H., et al.: MM-GTUNets: Unified multi-modal graph deep learning for brain disorders prediction. *IEEE Transactions on Medical Imaging* (2025)
30. Zeng, X., Gong, J., Li, W., Yang, Z.: Knowledge-driven multi-graph convolutional network for brain network analysis and potential biomarker discovery. *Medical Image Analysis* 99, 103368 (2025)

31. Tzourio-Mazoyer, N., Landeau, B., Papathanassiou, D., et al. : Automated anatomical labeling of activations in SPM using a macroscopic anatomical parcellation of the MNI MRI single-subject brain. *NeuroImage* 15(1), 273–289 (2002)
32. Laumann, T.O., Snyder, A.Z., Mitra, A. et al. : On the stability of BOLD fMRI correlations. *Cerebral Cortex* 27(10), 4719–4732 (2017)
33. Ying, Z., Bourgeois, D., You, J., Zitnik, M., Leskovec, J.: Gnnexplainer: Generating explanations for graph neural networks. *Advances in Neural Information Processing Systems* 32 (2019)
34. Silver, D., Huang, A., Maddison, C.J., et al.: Mastering the game of Go with deep neural networks and tree search. *Nature* 529(7587), 484–489 (2016)
35. Shan, C., Shen, Y., Zhang, Y., Li, X., Li, D.: Reinforcement learning enhanced explainer for graph neural networks. *Advances in Neural Information Processing Systems* 34, 22523–22533 (2021)